ADVANCED FUNCTIONAL MATERIALS
www.afm-journal.de

Coreless Fiber-Based Whispering-Gallery-Mode Assisted Lasing from Colloidal Quantum Well Solids

*Mustafa Sak, Nima Taghipour, Savas Delikanli, Sushant Shendre, Ibrahim Tanriover, Sina Foroutan, Yuan Gao, Junhong Yu, Zhou Yanyan, Seongwoo Yoo, Cuong Dang, and Hilmi Volkan Demir**

Whispering gallery mode (WGM) resonators are shown to hold great promise to achieve high-performance lasing using colloidal semiconductor nanocrystals (NCs) in solution phase. However, the low packing density of such colloidal gain media in the solution phase results in increased lasing thresholds and poor lasing stability in these WGM lasers. To address these issues, here optical gain in colloidal quantum wells (CQWs) is proposed and shown in the form of high-density close-packed solid films constructed around a coreless fiber incorporating the resulting whispering gallery modes to induce gain and waveguiding modes of the fiber to funnel and collect light. In this work, a practical method is presented to produce the first CQW-WGM laser using an optical fiber as the WGM cavity platform operating at low thresholds of ≈188 μJ cm^{-2} and ≈1.39 mJ cm^{-2} under one- and two-photon absorption pumped, respectively, accompanied with a record low waveguide loss coefficient of ≈7 cm^{-1} and a high net modal gain coefficient of ≈485 cm^{-1}. The spectral characteristics of the proposed CQW-WGM resonator are supported with a numerical model of full electromagnetic solution. This unique CQW-WGM cavity architecture offers new opportunities to achieve simple high-performance optical resonators for colloidal lasers.

1. Introduction

Colloidal semiconductor nanocrystals (NCs) have been considered as an excellent material platform for light amplification applications[1–5] thanks to their solution processability, low-cost production, and wide spectral tunability achieved by altering their shape, size, and composition.[6,7] Various shapes of the semiconductor NCs including colloidal quantum dots (CQDs),[1] nanorods (NRs),[8] colloidal quantum wells,[9,10] and perovskite nanocrystals[11,12] have been utilized as potent gain media for the optical gain and lasing applications. Among these nanocrystals, the colloidal quantum wells (CQWs), also known as nanoplatelets deserve a unique place considering their superior optical and electronic characteristics including giant oscillator strength,[13] exceptionally large linear and nonlinear absorption cross-sections,[14] purely homogeneous broadening,[15] and ultralarge modal optical gain coefficients.[16] In addition, the excitonic features of these atomically flat NCs can be tuned by using their heterostructures (i.e., core/crown[17–19] and core/shell[10,20,21]) which result in highly efficient optical gain performances.[3,10] Previously, various heterostructures of CQWs have been extensively used as gain media in optical gain and colloidal laser applications, in the close-packed solid film phase, integrated into different optical resonator structures. These specifically include vertical cavity surface-emitting lasers[9] and photonic-crystal nanobeam cavities.[22] Moreover, multiphoton-pumped lasing has been previously reported in the solution phase of CQWs by using a Fabry–Perot resonator.[23]

Recently, whispering gallery mode (WGM) resonators have proven to be highly promising optical cavities in optical amplification owing to their low optical losses.[24] WGM resonators have been made in the forms of microspheres,[25] microdisks,[26] and microrings[27] by virtue of the advanced and matured microfabrication techniques. As an alternative, fiber-based WGM resonators have been used as a cost-effective optical resonator for lasing in the solution phase of different colloidal fluorescent materials including organic dyes,[28] CQDs,[29,30] and NRs.[24] However, they mostly suffer from the low packing-density of such gain media in the dispersed solvents (e.g., hexane,

M. Sak, N. Taghipour, Dr. S. Delikanli, I. Tanriover, S. Foroutan, Prof. H. V. Demir
Department of Electrical and Electronics Engineering
Department of Physics
UNAM-Institute of Materials Science and Nanotechnology
Bilkent University
Ankara 06800, Turkey
E-mail: volkan@bilkent.edu.tr
Dr. S. Delikanli, Dr. S. Shendre, Dr. Y. Gao, Dr. J. Yu, Dr. Z. Yanyan, Prof. S. Yoo, Prof. C. Dang, Prof. H. V. Demir
LUMINOUS! Centre of Excellence for Semiconductor Lighting and Displays
Centre of Optical Fiber Technology
The Photonics Institute
School of Electrical and Electronic Engineering
School of Physical and Mathematical Sciences
Nanyang Technological University
50 Nanyang Avenue, Singapore 639798, Singapore
E-mail: hvdemir@ntu.edu.sg

The ORCID identification number(s) for the author(s) of this article can be found under https://doi.org/10.1002/adfm.201907417.

DOI: 10.1002/adfm.201907417

toluene, and chloroform), typically resulting in poor lasing stability and high lasing thresholds.[30] One way to overcome these issues is to employ close-packed films of colloidal NCs as a gain medium in fiber-based WGM resonators.

In the present work, we propose and develop a coreless fiber-based WGM-assisted laser of the high-density close-packed CQW solids that address the problems of increased lasing threshold and poor lasing stability as the first WGM-CQW lasing architecture. Here we demonstrate amplified spontaneous emission (ASE) and lasing in the close-packed film of our CdSe/CdS@$Cd_{1-x}Zn_xS$ core/crown@gradually alloyed shell (C/C@GAS) CQWs with one-photon-absorption (1PA) and two-photon-absorption (2PA) pumping sources. The laser structure consists of a novel coreless fiber-based WGM optical resonator which is also coupled to the waveguiding modes of the fiber. For this purpose, the close-packed films of these CQWs were formed as gain medium surrounding bare SiO_2 fibers conveniently using adhesion. In this work, we systematically studied the 1PA and 2PA pumped ASE performances of these CQW-WGM resonators in two selected core diameters of 125 and 250 μm. This unique CQW-WGM cavity allows us to achieve low ASE thresholds of ≈85.10 μJ cm^{-2} and ≈3.10 mJ cm^{-2} under 1PA and 2PA pumping, correspondingly, accompanied with a net high modal gain coefficient of ≈485 cm^{-1} and a record low waveguide loss coefficient of ≈7 cm^{-1}. Finally, as a proof-of-concept demonstration, we present a linearly polarized WGM-assisted laser from CQWs operating at a threshold of ≈188 μJ cm^{-2} under 1PA pumping with stable lasing emission under 150 min of continuous excitation.

2. Results and Discussion

In this study, we synthesized CdSe/CdS@$Cd_{1-x}Zn_xS$ C/C@GAS via a colloidal atomic layer deposition technique where $Cd_{1-x}Zn_xS$ shells were grown on the seed 4-monolayer (4-ML) CdSe/CdS core/crown CQWs.[20] Thanks to this specially engineered heterostructure of our CQWs, the electron wavefunction feels soft confinement potential in the vertical direction of the heterostructure owing to the small offset between the conduction bands of the core and gradually alloyed shell, while the hole wavefunction is mostly localized in the core region due to the large valence band offset.[31] This forms a quasi-type-II band structure, and the spatial overlap between the electron- and hole-wavefunctions is reduced in this system compared to the systems with type-I band alignment as previously demonstrated in CdSe/CdS dot/rod NCs.[8] Moreover, it has been previously shown that smoothening of the potential barrier effectively suppresses Auger recombination,[32] which was also theoretically predicted in the quantum-confined structures.[33] Owing to the soft confinement potential of electron wavefunction in our engineered hetero-CQWs, nonradiative Auger recombination is significantly suppressed.[31] High-angle annular dark-field scanning transmission electron microscopy (HAADF-STEM) image of the C/C@GAS shell CQWs with 3-MLs of gradient alloyed shells is given in **Figure 1**a,b. The core and shell regions of our C/C@GAS CQWs is marked in the high-resolution transmission electron microscopy image shown in Figure 1b. Figure 1c depicts the absorption and photoluminescence (PL) spectra of these CQWs. The PL spectrum of the CQWs is centered around 640 nm, and the heavy- and light-hole excitonic transitions are located at 630 and 575 nm, respectively, as can be seen in the absorption spectrum of these CQWs.

We prepared close-packed solid films of CdSe/CdS@$Cd_{1-x}Zn_xS$ C/C@GAS CQWs around two different coreless fibers with the diameters of 125 and 250 μm via employing adhesion to characterize optical gain performances of these CQWs. For construction of the fiber-based CQW-WGM resonator, as a simple and convenient method, the fibers were dipped into highly concentrated (60–70 mg mL^{-1}) hexane solution of CQWs (see the Experimental Section for details). Figure 1d shows the scanning electron microscopy (SEM) image of the high-density close-packed film solid films of our CQWs. As can been in Figure 1d, a close-packed film of CQWs covers the fiber surface. We performed amplified spontaneous emission measurement through 1PA and 2PA excitations (see the Experimental Section). By employing SEM technique, the thickness of the solid films around the fibers was measured to be ≈7 μm as shown in Figure 1d.

Figure 2a presents the pump-dependent PL spectra of the CQW-coated fiber with the core size of 250 μm under 1PA excitation as an exemplary case. As can be seen in Figure 2a, at low pump fluences the spontaneous emission dominates the PL spectra with a full-width-at-half-maximum (FWHM) of ≈25 nm. Then, as the pump intensity is further increased, an ASE peak appears at ≈642 nm with a narrower FWHM of ≈7 nm above the optical gain threshold. Figure 2b exhibits the integrated emission intensity of both of the CQW-coated fibers as a function of the 1PA pump fluences, where the ASE thresholds of CQW-coated fibers were found as ≈85.10 μJ cm^{-2} and ≈131.10 μJ cm^{-2} for 250 and 125 μm diameter fibers, respectively.

Furthermore, we investigated 2PA-pumped ASE performances of these CQW-fibers. The luminescence spectra of the one with the core diameter of 250 μm under 2PA are given in Figure 2c. The appearance of ASE peak is clearly seen in Figure 2c for excitation fluences above the gain threshold, where spectral narrowing (FWHM of ≈7 nm) occurs in the emission along with an abrupt rise in the integrated intensity (Figure 2d). As shown in Figure 2d, below the gain threshold the integrated intensity follows a linear function of the excitation fluence, where spontaneous emission covers the PL spectra. Subsequently, above the ASE threshold the integrated intensity follows a superlinear behavior. The resulting ASE thresholds were measured as ≈3.10 and ≈4.50 mJ cm^{-2} for 250 and 125 μm diameter fibers, respectively. It can be seen that the ASE thresholds are significantly decreased for both 1PA and 2PA pumped regimes as the diameter of the fiber is increased from 125 to 250 μm. We attribute this behavior to the difference in waveguide loss coefficients, which will be analyzed and discussed in detail later in the paper.

To further investigate the optical gain performance of these CQW-coated-fibers, we characterized the net modal gain coefficients by employing variable stripe length (VSL) method. To do so, luminescence spectra of the samples were recorded as a function of the beam stripe length at a fixed pump fluence under 1PA excitation (see the Supporting Information). The luminescence spectra of one CQW-coated fiber (250 μm)

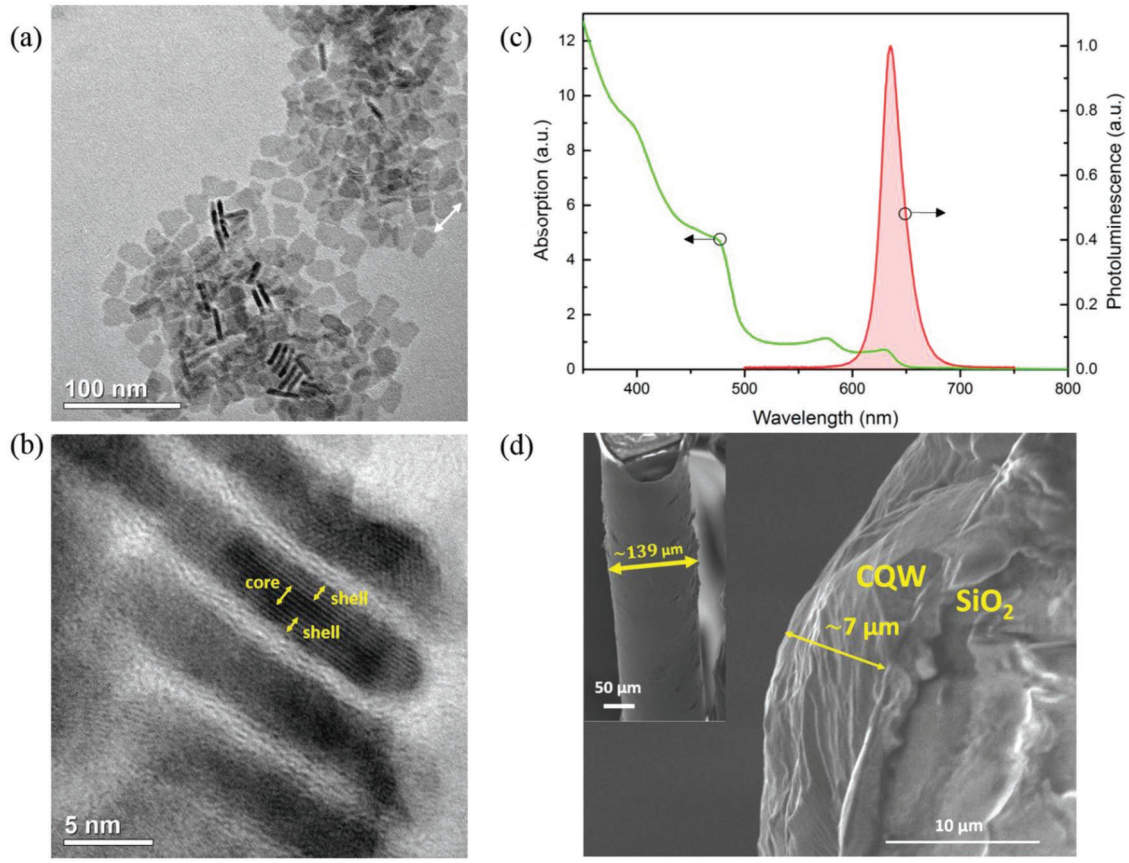

Figure 1. a,b) High-angle annular dark-field scanning transmission electron microscopy (HAADF-STEM) image to demonstrate the thickness of CdSe/CdS@$Cd_{1-x}Zn_xS$ (C/C@GAS) CQWs. c) Absorption and photoluminescence spectra of C/C@GAS CQWs. d) Scanning electron microscopy (SEM) image of CQW-coated fiber to show high packing density. The inset depicts the overall thickness of the fiber (125 µm) along with close-packed solid CQW film.

are shown in **Figure 3**a for various stripe lengths at a pump fluence of 247 µJ cm^{-2}. Similar to ASE measurements, a red-shifted narrow emission emerges above a certain length of the stripe. Figure 3b represents the integrated PL intensity of the fiber with 250 µm diameter as a function of the stripe length at various pump fluences. Then, the net modal gain coefficients were quantified by fitting the experimental data to the following expression

$$I(l) = I_{sp}\frac{\left(e^{Gl}-1\right)}{G} \quad (1)$$

Here, $I(l)$ is the integrated intensity of the PL spectra, l is the stripe length, I_{sp} is a proportionality constant, which is related to the spontaneous emission, and G is the net modal gain coefficient. The calculated G is plotted as a function of the excitation fluence in Figure 3c, and subsequently, G values are fitted to the following equation

$$G = g - \alpha = \Gamma \times \sigma_{st} \times \frac{\Phi_p}{1+\frac{\Phi_p}{\Phi_s}} \quad (2)$$

where G is the net modal gain, g is the peak modal gain, α is the total loss of the system, σ_{st} is the stimulated emission absorption cross-section, Γ is the optical mode confinement factor, Φ_p is the pump fluence, and Φ_s is the saturation pump fluence. As shown in Figure 3c, the net modal gain follows a linear function at low pump fluences and a progressive saturation appears at raised pump fluences. The largest G was experimentally achieved as high as 485 cm^{-1} for the pump fluence of 585 µJ cm^{-2}, while based on the numerical fitting, through Equation (2), Φ_s was found as ≈900 µJ cm^{-2}.

Next, we examined the waveguide loss coefficients of the CQW-coated fibers. For this purpose, we measured the ASE peak intensity of the samples as a function of the distance from the edge of the samples (see the Supporting Information). Then, to quantify the waveguide loss coefficients, the experimental data were fitted to the exponential function of $I(l) = I_0\, e^{-\alpha l}$, where I_0 is the ASE peak intensity, l is the distance from the edge of the fiber to end of the stripe, and α is the waveguide loss coefficient. From the numerical fitting, α was found to be as low as 11.25 ± 0.53 and 7.08 ± 0.38 cm^{-1} for 125 and 250 µm diameter fibers, respectively (see Figure 3d). Our findings for α are the lowest reported waveguide loss coefficient compared to the previously reports using all-solution-processed materials including CQWs,[3,34] and CQDs.[35] The ratio between the loss coefficients of 125 and 250 µm diameter fibers is found as 1.59, which correlates to the ratio of ASE their thresholds (1.54). This simple but significant correlation between these ratios

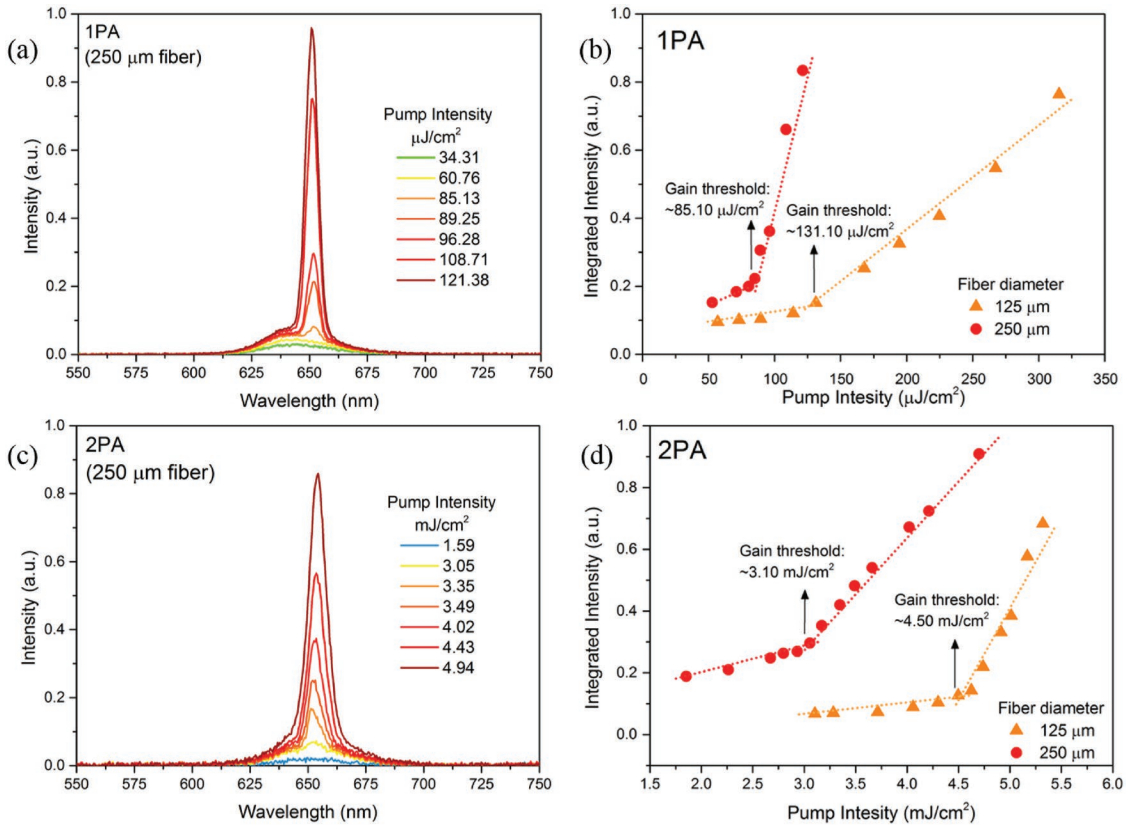

Figure 2. a) PL spectra of CQW-coated 250 μm diameter fiber under 1PA excitation. b) Integrated intensity as a function of the pump intensity under 1PA for both CQW-fibers with different diameters (125 and 250 μm). c) PL spectra of the 250 μm diameter CQW-fiber under 2PA excitation. d) Integrated intensity as a function of the pump intensity under 2PA excitation for both fibers (125 and 250 μm).

may create a platform for optical gain studies with predictable characteristics.

In our proposed architecture, whispering gallery modes are supported in the gain medium because the refractive index of the gain medium (n_{CQW} = 1.80) which is higher than the surrounding media, air (n_{air} = 1), and silica (n_1 = 1.46) (see **Figure 4**a), resulting in total internal reflections occurring at the interfaces of the CQW-air and CQW-SiO_2. This allows to construct a unique CQW-WGM cavity, where the generated omnidirectional light from the gain medium is funneled and guided to the end of the fiber by coupling into the waveguiding modes of the fiber. Here, we show multimode lasing in this CQW-WGM resonator by utilizing a spot excitation geometry (with the fiber diameter of 250 μm) as a proof-of-concept demonstration. The illustrated schematic in Figure 4a displays the cross-section of the fiber, which functions as a WGMs resonator. As can be seen in Figure 4a, the coating of the CQWs solid film on the surface of the fiber is nonuniform. This results in a medium with an effective refractive index value between n_{air} and n_{CQW}. The emission spectra from the CQW-WGM structure at different pump intensities are presented in Figure 4b, showing a sharp multimode laser output with an FWHM of ≈1.35 nm, which corresponds to one of the WGM modes of the resonator. Pump fluence dependent lasing emission is shown in Figure 4c, where the lasing threshold of 188 μJ cm^{-2} can be seen with a characteristic S-curve profile of the lasing emission displaying gradual saturation at the elevated pumps. The coherent laser emission of the CQW-WGM resonator is depicted in Figure 4d with a well-defined laser spot. It is worth noting that this laser spot is the emission of our CQW-WGM resonator, which is coupled to the waveguiding modes of the SiO_2 fiber. Even though the emission of a WGM resonator is omnidirectional, we can effectively guide this emission along the length of the SiO_2 fiber to its end thanks to the strong waveguiding behavior of the bare fiber.

Additionally, we examined the lasing performance of CQW-WGM resonator under 2PA excitation for possible applications of this structure in nonlinear photonics including biosensing[36] and upconverted colloidal lasers.[37] The lasing threshold under 2PA pumping was found to be 1.39 mJ cm^{-2} as presented in Figure 4e,f. The obtained lasing thresholds under 1PA- and 2PA-pumping are comparable to or lower than the previously reported best lasing thresholds from WGM resonators based on high-performance engineered heterostructures of solution-processed semiconductor NCs including CQD-based (CdSe/CdZnS/ZnS, CdZnS/ZnS, CdSe/ZnS, and CdZnS/ZnS),[30,38–40] nanorod-based (CdSe/ZnS),[24] and CQW-based (CdSe/CdS)[23] lasers. We attribute the high performance of this CQW-WGM laser to the close-packed solid film phase formation of our CQWs around the fiber while all of the previous reports are based on the solution phase (dispersion) of colloidal semiconductor NCs[29] or on the microbubble formation.[39] This

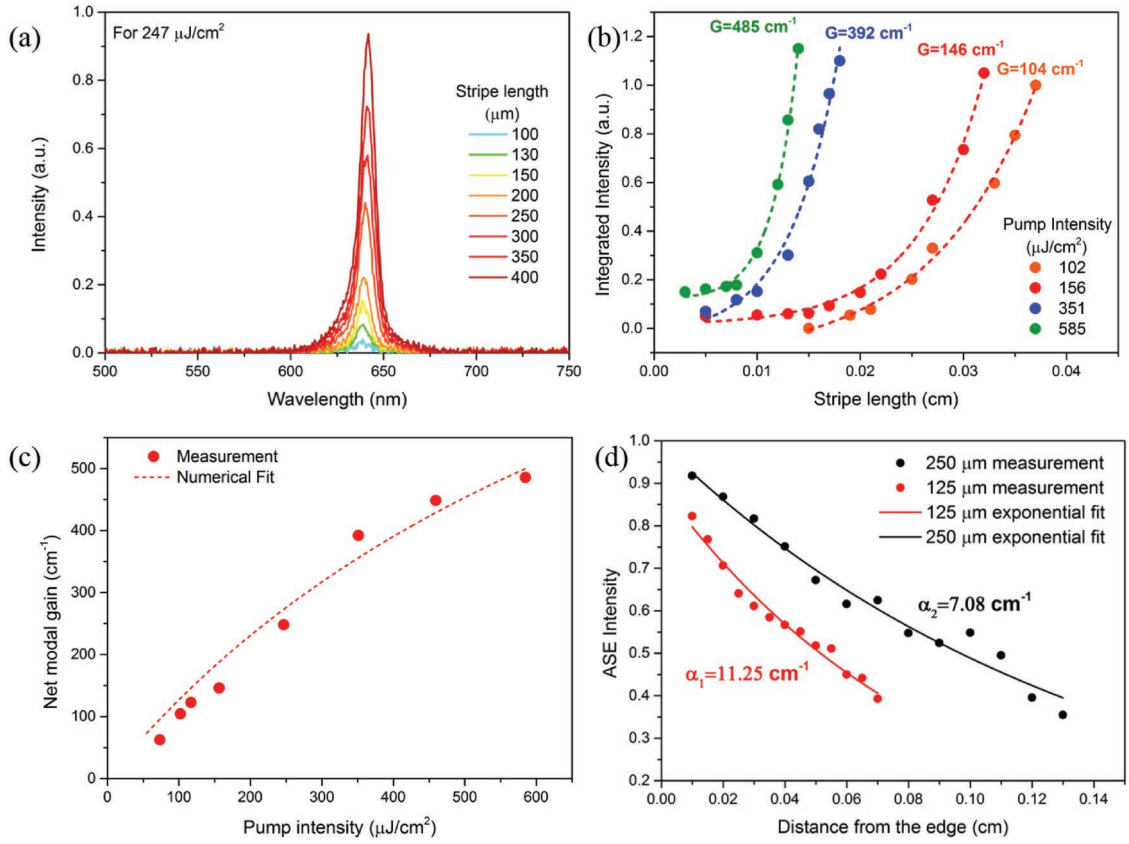

Figure 3. a) ASE spectra of CQW-coated 250 μm diameter fiber under 1PA excitation for various stripe lengths at pump fluence of 246 μJ cm^{-2}. b) Variable stripe length (VSL) measurement of CQW-coated 250 μm diameter fiber for different pump intensities. c) Net modal gain (G) coefficient as a function of pump fluence. d) ASE intensity as a function of distance from the edge to calculate waveguide loss coefficient (α) of the fibers under 1PA excitation.

close-packed high-density formation of the CQWs, together with significantly low scattering losses, result in extraordinarily low optical waveguide loss coefficients while achieving high modal gain coefficients, and consequently substantially reduced thresholds in the proposed CQW-WGM laser.

To better understand the multimode lasing behavior of our CQW-WGM structure, we performed a full electromagnetic solution using finite difference time-domain method via a commercial software package (Lumerical finite-difference time-domain Solutions). The results of our numerical modeling are presented in **Figure 5**a, which show that the electric field is strongly localized in the solid film region of CQWs around the fiber. In our numerical simulations, we modeled the gain media with an optical refractive index (n_{CQW}) of 1.80 according to our experimental characterization via ellipsometry technique. This strong electric field confinement in gain medium occurs thanks to the strong total internal reflections at the interfaces of CQW with air and SiO_2 (see the Supporting Information for details).

Moreover, we investigated the funneling of our CQW-WGM emission to the guided modes of the coreless fiber by performing a full 3D electromagnetic simulation of our CQW-WGM structure (see the Supporting Information). Due to the large size of our structure (orders of mm in length), we scaled down our structure by tenfold in all dimensions to obtain a reasonable computation time; otherwise, the simulation of such a large structure also requires a huge amount of memory. As a result, for a smooth CQW film surface, the emission is mostly confined within the CQW film region as can be seen in Figure 5a,b. Then, based on the SEM images of our CQW-coated coreless fibers, we introduced surface roughness to our simulated structure. Figure 5c represents the electric field distribution along the optical fiber for the rough surface, where it can be seen that this roughness results in significant optical scattering of the emitted light in our CQW-WGM resonator (see the Supporting Information for details). This enhances the leakage of the confined electric field in the CQW film region. Thus, the generated omnidirectional WGMs in our structure coupled to the waveguiding modes of optical fiber, utilize the guiding of WGM emission through the coreless fiber axis. It is worth mentioning that the delocalization of the electric field from CQW film to the SiO_2 and air region significantly lowers the effective refractive index of our structure.

Furthermore, to find the corresponding theoretical angular mode numbers of WGM in our structure, we employed the expression of $m\ \lambda_m = n_{eff}\ \pi D$, where m is the angular mode number, λ_m is the corresponding wavelength of the mth mode, n_{eff} is the effective refractive index of CQW film, and D is the diameter of structure.[41] We assume that the observed multimode lasing peaks in our experimental measurement correspond to the consecutive angular modes of the CQW-WGM resonator. As a

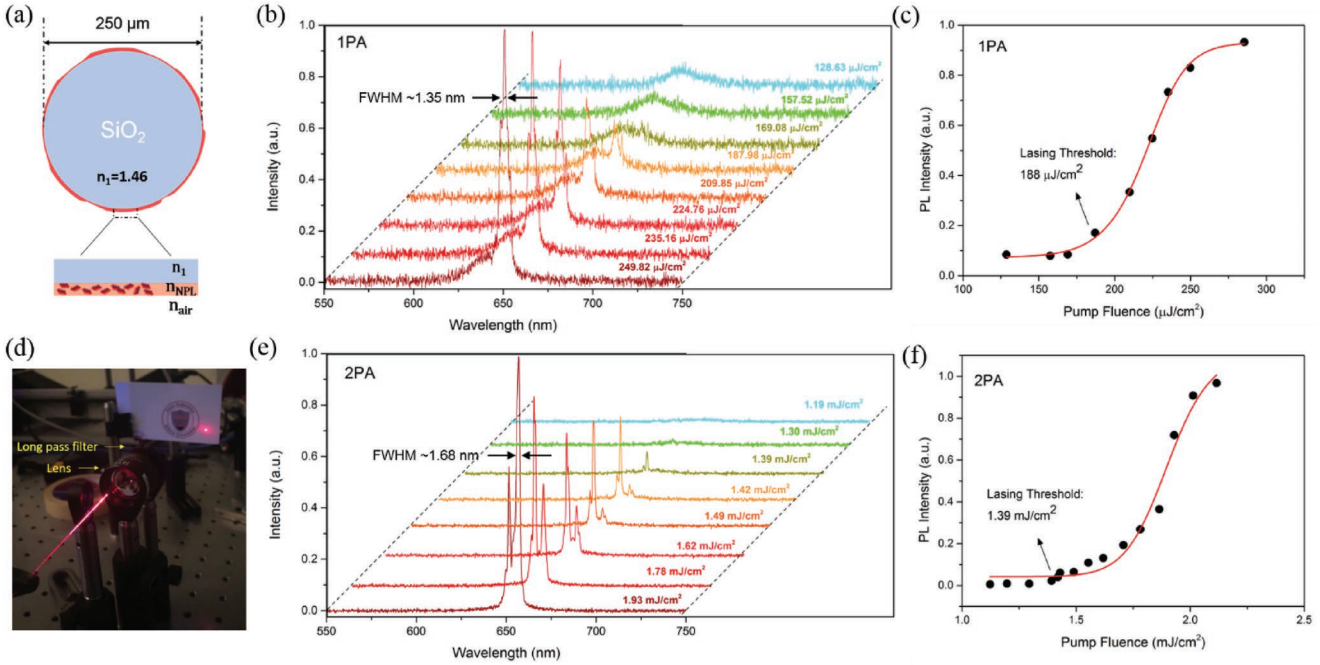

Figure 4. a) Schematic illustration of the cross-section for the CQW-integrated fiber. b) Luminescence spectra of 250 μm diameter CQW-fiber under 1PA excitation. c) Pump fluence dependent PL intensity for 1PA excitation. d) Image of the resulting laser spot from the optically excited fiber. e) Luminescence spectra of the 250 μm diameter CQW-fiber under 2PA excitation. f) Pump fluence dependent PL intensity for 2PA excitation.

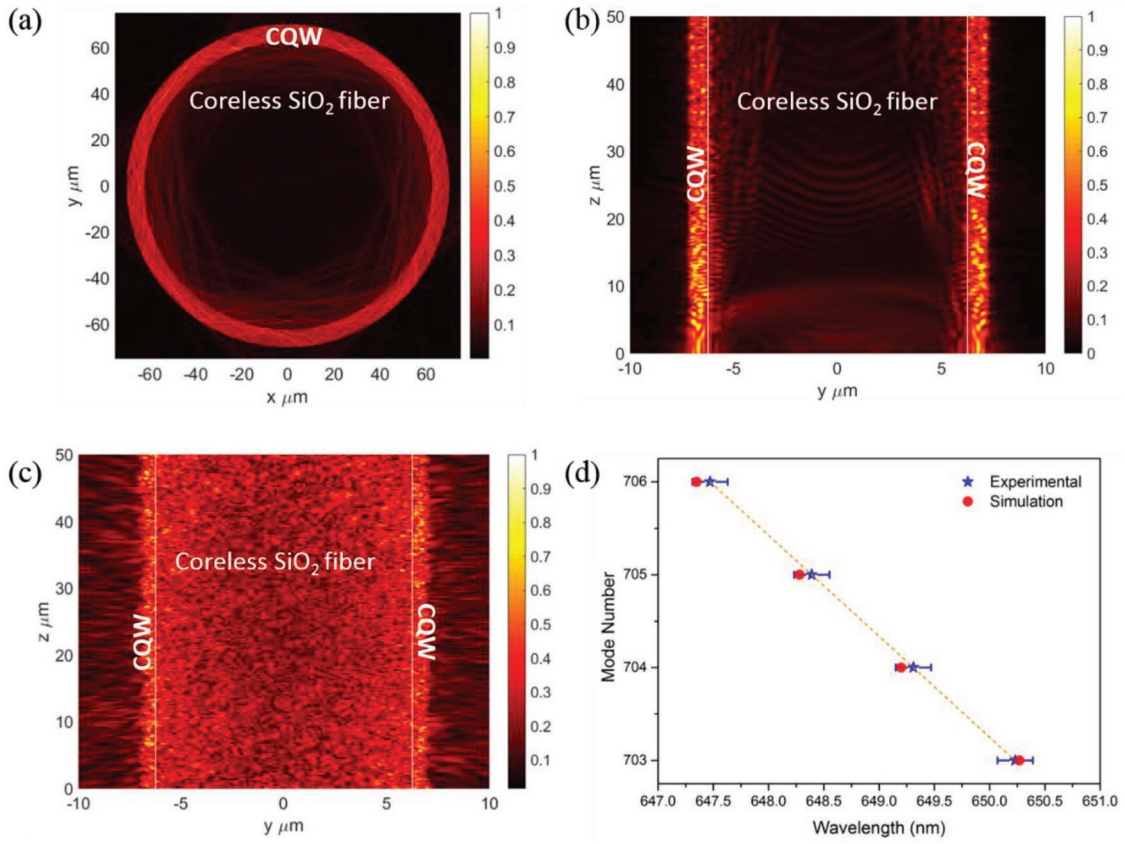

Figure 5. a) Electric field distribution for a 125 μm diameter fiber. b) Electric field distribution along the waveguiding direction of CQW film at the center of the coreless SiO_2 fiber for film with smooth surface and c) with rough surface. d) Lasing peaks of 125 μm diameter showing the experimentally measured and numerically simulated results.

result, the refractive index of the effective media (n_{eff}) was found to be ≈1.13. Figure 5d depicts the experimental and simulated peaks along with the corresponding theoretical angular mode number. Here the experimental measurements are in good agreement with our numerical results. It is worth to mention that we performed the numerical simulations and the mode analysis on the CQW-coated fiber with 125 µm diameter only. Since free spectral range (FSR) of a WGM resonator is inversely proportional to its diameter, FSR goes beyond the resolution of our spectrometer for the CQW-coated fiber with 250 µm diameter, and thus we cannot analyze the lasing modes for lasing measurements performed on the 250 µm diameter fiber using our available equipment.

To investigate the polarization state of our CQW-WGM laser output, the PL intensity was also recorded as a function of the linear polarizer angle, which was placed between the laser output and the spectrometer at a fixed pump fluence. Subsequently, the obtained experimental data were fitted with a quadratic cosine function as shown in **Figure 6**a. The

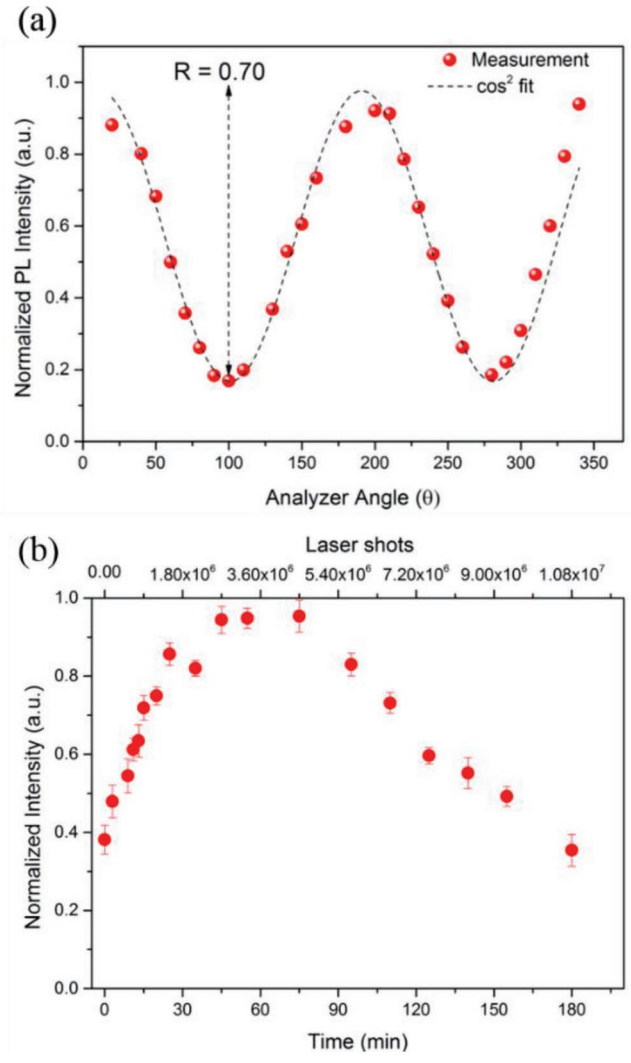

Figure 6. a) Normalized laser intensity as a function of the polarizer angle for CQW-WGM laser. b) Normalized laser intensity under continuously pumped excitation.

factor of the polarization state was calculated via the following expression[42]

$$R = \frac{I_{\parallel} - I_{\perp}}{I_{\parallel} + I_{\perp}} \tag{3}$$

where $I_{\parallel}$ and $I_{\perp}$ correspond to the laser intensities parallel and perpendicular to the optical axis (in line with the fiber axis), respectively. By employing Equation (3), R was found to be 0.70 indicating a highly linearly polarized laser output from our CQW-WGM resonator. Then, we examined the stability of the WGM lasing by performing continuous pumping at a fixed pump intensity (fourfold greater than the lasing threshold). As depicted in Figure 6b, the lasing emission is stable up to nearly 150 min (9×10^6 laser shots under 1 kHz reputation rate) of continuous excitations (where the intensity drops to half of its peak). A related point worth noting is observation of the increase in the ASE peak within the first 30 min, which we attribute to the previously reported phenomenon of annealing our CQWs.[43] This high stability of the CQW laser emission can be attributed to the stability of the solid film formation of these CQWs surrounding the fiber, which is significantly longer than the previously reported WGM lasers based on CQDs.[29,44]

3. Conclusion

In conclusion, we introduced a coreless fiber-based WGM-assisted resonator architecture enabled by the close-packed films of C/C@GAS CQWs constructed using a simple coating technique. The high packing density of the resulting solid CQW films, combined with the specially engineered advanced heterostructure of these CQWs, enables a high net modal gain of ≈485 cm^{-1} along with a record low waveguide loss coefficient of ≈7 cm^{-1}, which together results in low ASE threshold values of 85.10 µJ cm^{-2} and 3.10 mJ cm^{-2} under 1PA and 2PA pumping, respectively. As a proof-of-concept demonstration, we also developed a 1PA- and 2PA-pumped WGM laser of these CQW solids having low respective thresholds of ≈188 µJ cm^{-2} and 1.39 mJ cm^{-2}, by means of which linearly polarized and highly stable laser emission is achieved. Regarding its high-performance results, effortless fabrication technique and spectral tunability, the proposed CQW-WGM resonator is an excellent candidate for a wide range of applications including biosensing and biophotonics.

4. Experimental Section

Sample Preparation: To form high-density close-packed solid films of CdSe/CdS@$Cd_{1-x}Zn_xS$ C/C@GAS CQWs around the glass fiber, a highly concentrated solution (60–70 mg mL^{-1}) of the CQWs was prepared in hexane. Then, bare fibers (125 and 250 µm diameter) were dipped into the solution, thanks to adhesion, after 30–40 min, a thick layer of the CQWs was coated around the fiber.

ASE Measurement: Mode-locked Ti:Sapphire laser was used as the pumping source with a repetition rate of 1 kHz, a pulse width of 120 fs at 800 nm (2PA) or at 400 nm (1PA) employing a frequency-doubled via a beta barium borate crystal). For ASE measurements, a cylindrical lens was employed to obtain stripe geometry. A neutral density filter was placed to adjust the pump intensities on the samples. Then, the

emission of the sample was collected via Maya 2000 Pro spectrometer at the end of the fiber.

Supporting Information

Supporting Information is available from the Wiley Online Library or from the author.

Acknowledgements

M.S. and N.T. contributed equally to this work. The authors gratefully acknowledge the financial support in part from Singapore National Research Foundation under the programs of NRF-NRFI2016-08 and the Science and Engineering Research Council, Agency for Science, Technology and Research (A*STAR) of Singapore and in part from TUBITAK 114F326 and 115E679. H.V.D. also acknowledges support from TUBA. M.S. and I.T. acknowledge support from TUBITAK BIDEB.

Conflict of Interest

The authors declare no conflict of interest.

Keywords

laser, nanoplatelets, optical gain, waveguiding, whispering-gallery-mode

Received: September 7, 2019
Revised: September 28, 2019
Published online: November 4, 2019

[1] V. I. Klimov, A. A. Mikhailovsky, J. A. Hollingsworth, A. Malko, C. A. Leatherdale, H. J. Eisler, M. G. Bawendi, *Science* **2000**, *290*, 314.
[2] K. Wu, Y. S. Park, J. Lim, V. I. Klimov, *Nat. Nanotechnol.* **2017**, *12*, 1140.
[3] D. Dede, N. Taghipour, U. Quliyeva, M. Sak, Y. Kelestemur, K. Gungor, H. V. Demir, *Chem. Mater.* **2019**, *31*, 1818.
[4] P. Brenner, O. Bar-On, M. Jakoby, I. Allegro, B. S. Richards, U. W. Paetzold, I. A. Howard, J. Scheuer, U. Lemmer, *Nat. Commun.* **2019**, *10*, 988.
[5] C. D. Sonnichsen, T. Kipp, X. Tang, P. Kambhampati, *ACS Photonics* **2019**, *6*, 382.
[6] D. V. Talapin, J. Lee, M. V. Kovalenko, E. V. Shevchenko, **2010**, *110*, 389.
[7] J. M. Pietryga, Y. S. Park, J. Lim, A. F. Fidler, W. K. Bae, S. Brovelli, V. I. Klimov, *Chem. Rev.* **2016**, *116*, 10513.
[8] M. Saba, S. Minniberger, F. Quochi, J. Roither, M. Marceddu, A. Gocalinska, M. V. Kovalenko, D. V. Talapin, W. Heiss, A. Mura, G. Bongiovanni, *Adv. Mater.* **2009**, *21*, 4942.
[9] B. Guzelturk, Y. Kelestemur, M. Olutas, S. Delikanli, H. V. Demir, *ACS Nano* **2014**, *8*, 6599.
[10] C. She, I. Fedin, D. S. Dolzhnikov, A. Demortière, R. D. Schaller, M. Pelton, D. V. Talapin, *Nano Lett.* **2014**, *14*, 2772.
[11] S. Yakunin, L. Protesescu, F. Krieg, M. I. Bodnarchuk, G. Nedelcu, M. Humer, G. De Luca, M. Fiebig, W. Heiss, M. V. Kovalenko, *Nat. Commun.* **2015**, *6*, 1.
[12] Y. Wang, X. Li, X. Zhao, L. Xiao, H. Zeng, H. Sun, *Nano Lett.* **2016**, *16*, 448.
[13] S. Ithurria, M. D. Tessier, B. Mahler, R. P. S. M. Lobo, B. Dubertret, A. L. Efros, *Nat. Mater.* **2011**, *10*, 936.
[14] M. Olutas, B. Guzelturk, Y. Kelestemur, A. Yeltik, S. Delikanli, H. V. Demir, *ACS Nano* **2015**, *9*, 5041.
[15] M. D. Tessier, C. Javaux, I. Maksimovic, V. Loriette, B. Dubertret, *ACS Nano* **2012**, *6*, 6751.
[16] B. Guzelturk, M. Pelton, M. Olutas, H. V. Demir, *Nano Lett.* **2019**, *19*, 277.
[17] M. D. Tessier, P. Spinicelli, D. Dupont, G. Patriarche, S. Ithurria, B. Dubertret, *Nano Lett.* **2014**, *14*, 207.
[18] S. Delikanli, B. Guzelturk, P. L. Hernández-Martínez, T. Erdem, Y. Kelestemur, M. Olutas, M. Z. Akgul, H. V. Demir, *Adv. Funct. Mater.* **2015**, *25*, 4282.
[19] Y. Gao, M. Li, S. Delikanli, H. Zheng, B. Liu, C. Dang, T. C. Sum, H. V. Demir, *Nanoscale* **2018**, *10*, 9466.
[20] S. Shendre, S. Delikanli, M. Li, D. Dede, Z. Pan, S. T. Ha, Y. H. Fu, P. L. Hernández-Martínez, J. Yu, O. Erdem, A. I. Kuznetsov, C. Dang, T. C. Sum, H. V. Demir, *Nanoscale* **2019**, *11*, 301.
[21] F. Muckel, S. Delikanli, P. L. Hernández-Martínez, T. Priesner, S. Lorenz, J. Ackermann, M. Sharma, H. V. Demir, G. Bacher, *Nano Lett.* **2018**, *18*, 2047.
[22] Z. Yang, M. Pelton, I. Fedin, D. V. Talapin, E. Waks, *Nat. Commun.* **2017**, *8*, 143.
[23] M. Li, M. Zhi, H. Zhu, W. Y. Wu, Q. H. Xu, M. H. Jhon, Y. Chan, *Nat. Commun.* **2015**, *6*, 1.
[24] M. Kazes, D. Y. Lewis, Y. Ebenstein, T. Mokari, U. Banin, *MRS Proc.* **2011**, *789*, 317.
[25] J. Ward, O. Benson, *Laser Photonics Rev.* **2011**, *5*, 553.
[26] T. J. Kippenberg, J. Kalkman, A. Polman, K. J. Vahala, *Phys. Rev. A* **2006**, *74*, 51802.
[27] M. Kuwata-Gonokami, S. Ozawa, R. H. Jordan, A. Dodabalapur, H. E. Katz, M. L. Schilling, R. E. Slusher, *Opt. Lett.* **1995**, *20*, 2093.
[28] S. I. Shopova, H. Zhou, X. Fan, P. Zhang, *Appl. Phys. Lett.* **2007**, *90*, 221101.
[29] A. Kiraz, Q. Chen, X. Fan, *ACS Photonics* **2015**, *2*, 707.
[30] Y. Wang, K. S. Leck, D. Van Ta, R. Chen, V. Nalla, Y. Gao, T. He, H. V. Demir, H. Sun, *Adv. Mater.* **2015**, *27*, 169.
[31] N. Taghipour, S. Delikanli, S. Shendre, M. Sak, M. Li, F. Isik, I. Tanriover, B. Guzelturk, T. C. Sum, H. V. Demir, *arXiv* **2019**, 1906.06913.
[32] W. K. Bae, L. A. Padilha, Y. S. Park, H. McDaniel, I. Robel, J. M. Pietryga, V. I. Klimov, *ACS Nano* **2013**, *7*, 3411.
[33] G. E. Cragg, A. L. Efros, *Nano Lett.* **2010**, *10*, 313.
[34] B. Guzelturk, Y. Kelestemur, M. Olutas, Q. Li, T. Lian, H. V. Demir, *J. Phys. Chem. Lett.* **2017**, *8*, 5317.
[35] C. H. Lin, E. Lafalce, J. Jung, M. J. Smith, S. T. Malak, S. Aryal, Y. J. Yoon, Y. Zhai, Z. Lin, Z. V. Vardeny, V. V. Tsukruk, *ACS Photonics* **2016**, *3*, 647.
[36] R. N. Day, W. Tao, K. W. Dunn, *Nat. Protoc.* **2016**, *11*, 2066.
[37] B. Guzelturk, Y. Kelestemur, K. Gungor, A. Yeltik, M. Z. Akgul, Y. Wang, R. Chen, C. Dang, H. Sun, H. V. Demir, *Adv. Mater.* **2015**, *27*, 2741.
[38] N. Zhang, H. Liu, A. M. Stolyarov, T. Zhang, K. Li, P. P. Shum, Y. Fink, X. W. Sun, L. Wei, *ACS Photonics* **2016**, *3*, 2275.
[39] Y. Wang, V. D. Ta, K. S. Leck, B. H. I. Tan, Z. Wang, T. He, C. D. Ohl, H. V. Demir, H. Sun, *Nano Lett.* **2017**, *17*, 2640.
[40] J. P. Mondia, R. Sharma, Z. H. Lu, A. S. Susha, A. L. Rogach, L. J. Wang, J. Schäfer, *Nano Lett.* **2008**, *8*, 1709.
[41] H. H. Fang, R. Ding, S. Y. Lu, Y. De Yang, Q. D. Chen, J. Feng, Y. Z. Huang, H. B. Sun, *Laser Photonics Rev.* **2013**, *7*, 281.
[42] J. Hu, L. S. Li, W. Yang, L. Manna, L. W. Wang, A. P. Alivisatos, *Science* **2001**, *292*, 2060.
[43] Y. Kelestemur, B. Guzelturk, O. Erdem, M. Olutas, K. Gungor, H. V. Demir, *Adv. Funct. Mater.* **2016**, *26*, 3570.
[44] P. T. Snee, Y. Chan, D. G. Nocera, M. G. Bawendi, *Adv. Mater.* **2005**, *17*, 1131.